Coarsening dynamics of nonequilibrium chiral Ising models

Mina Kim (김민아),[1] Su-Chan Park (박수찬),[2] and Jae Dong Noh (노재동)[1,3]
[1]*Department of Physics, University of Seoul, Seoul 130-743, Korea*
[2]*Department of Physics, The Catholic University of Korea, Bucheon 420-743, Korea*
[3]*School of Physics, Korea Institute for Advanced Study, Seoul 130-722, Korea*
(Received 5 October 2012; published 22 January 2013)

We investigate a nonequilibrium coarsening dynamics of a one-dimensional Ising spin system with chirality. Only spins at domain boundaries are updated so that the model undergoes a coarsening to either of equivalent absorbing states with all spins + or −. Chirality is imposed by assigning different transition rates to events at down (+−) kinks and up (−+) kinks. The coarsening is characterized by power-law scalings of the kink density $\rho \sim t^{-\delta}$ and the characteristic length scale $\xi \sim t^{1/z}$ with time t. Surprisingly the scaling exponents vary continuously with model parameters, which is not the case for systems without chirality. These results are obtained from extensive Monte Carlo simulations and spectral analyses of the time evolution operator. Our study uncovers the novel universality class of the coarsening dynamics with chirality.

DOI: 10.1103/PhysRevE.87.012129 PACS number(s): 05.50.+q, 02.50.Ey, 05.70.Ln

Coarsening takes place in various systems such as magnetic systems, binary alloys, and social systems with opinion dynamics. When a system is quenched from a high-temperature disordered phase to a low-temperature ordered phase, a typical size of domains grows in time following a power law,

$$\xi \sim t^{1/z}, \tag{1}$$

with dynamic exponent z. It is known that coarsening systems are classified into a few universality classes depending on spatial dimensionality, order parameter symmetry, conservation in dynamics, and so on [1].

The Ising model is one of the best studied coarsening systems. It is symmetric under the global spin inversion (Z_2 symmetry) and has a scalar order parameter. Under the single-spin-flip Glauber dynamics [2] that does not conserve the order parameter, the coarsening dynamics is characterized by $z = 2$. On the other hand, the dynamic exponent is given by $z = 3$ under the spin-exchange Kawasaki dynamics [3] conserving the order parameter. Systems with nonscalar order parameter constitute distinct universality classes [1].

A coarsening process is rather simple in systems with discrete symmetry and nonconserving dynamics in one dimension. Consider a one-dimensional (1D) Ising spin chain with the Glauber dynamics at zero temperature, or equivalently the voter model [4]. In this model, only spins at domain boundaries can flip so that domain walls diffuse and annihilate in pairs. The diffusive nature suggests that the dynamic exponent is given by $z = 2$ and that the domain wall density decays algebraically as

$$\rho \sim t^{-\delta}, \tag{2}$$

with an exponent $\delta = 1/2$. These scaling laws are verified by the exact solution [2,5,6].

The power-law scaling with $z = 2$ and $\delta = 1/2$ seems to be robust in one dimension. The q-state Potts model with the zero-temperature Glauber dynamics exhibits the same scaling behavior [5,7–9]. It is also observed in nonequilibrium systems. Consider the voter model with an additional exchange process of neighboring spins [10]. It is equivalent to the branching annihilating random walk (BAW) model [11,12], where domain walls diffuse, annihilate in pairs, and branch two offsprings. Despite the branching, the model displays the coarsening with the same exponents [12,13]. The voter model with a kinetic constraint also displays the same scaling behavior with a logarithmic correction [14].

Most studies on the coarsening have focused on the role of order parameter symmetry [1]. On the other hand, some dynamical systems are characterized by coupled symmetry and little is known about the coarsening dynamics in such systems. In this paper, we investigate the coarsening dynamics of a 1D Ising spin system which is invariant under the simultaneous inversion of spin and space. Remarkably, the model with the coupled symmetry constitutes a novel universality class that is characterized by continuously varying exponents.

Initial motivation of this work was to study a one-dimensional version of the flocking model introduced by Vicsek *et al.* [15] (Vicsek model, or VM for short). In the VM, the motion of each particle i at position $\boldsymbol{r}_i$ is described by a velocity vector $\boldsymbol{v}_i$ of a constant speed. Each time step, the direction of $\boldsymbol{v}_i$ is updated to the average direction of particles within a fixed distance perturbed by a random noise. The system coarsens into a flocking phase when the noise strength is small [15,16]. Note that spatial isotropy is broken spontaneously due to the motion of particles. Consequently, the model is *chiral*, i.e., symmetric under the simultaneous rotation/inversion of the velocity and the space.

In a 1D chain, the velocity of a self-propelled particle is restricted to be one of +1 or −1, once the speed of each particle remains constant just like the VM. Particles are assumed to see only along the direction it moves and the range of sight is limited to be 1. This one-dimensional system may be realized by the motion of myopic ants along a pheromone trail [17,18]. If a right-moving ant meets a left-moving one, both ants either align to the same direction or just pass each other.

This model can be represented by an Ising spin system $\{\boldsymbol{\sigma} = (\sigma_1, \ldots, \sigma_N)\}$ with velocity $\sigma_i = \pm 1$ in a 1D lattice of N sites under periodic boundary conditions. Here we assume that the density of particles is 1, but the generalization to systems with smaller density is straightforward. In terms of the Ising spins, the VM-like interaction in one dimension can

be represented by the following update rule:

$$+- \xrightarrow{u} -+, \qquad -+ \xrightarrow{\bar{u}} +-,$$
$$+- \xrightarrow{v/2} \begin{cases} ++, \\ --, \end{cases} \qquad -+ \xrightarrow{\bar{v}/2} \begin{cases} ++, \\ --, \end{cases} \tag{3}$$

where parameters over the arrows denote the transition rates of corresponding events. For theoretical reason, we also introduced the interaction of a local configuration $-+$. Without losing generality, we will set $u + v = 1$ and $\bar{u} + \bar{v} \leqslant 1$.

Our model is characterized by the chirality: The transition rates for events associated with down kinks ($+-$ pairs) and up kinks ($-+$ pairs) are different. This chirality breaks the Z_2 symmetry, but leaves system invariant under the simultaneous inversion of spin and space, $\sigma_i \to -\sigma_{-i}$. Emphasizing the role of the chirality, the model will be referred to as the nonequilibrium chiral Ising model (NCIM). The chirality is irrelevant for equilibrium Ising systems [19]. However, it turns out to result in an interesting feature in nonequilibrium cases.

The NCIM reduces to the voter model when $v = \bar{v}$ and $u = \bar{u} = 0$, and the asymmetric simple exclusion process (ASEP) [4] when $v = \bar{v} = 0$. A mixture of them was studied in Refs. [20,21] and was found to display complicated scaling behaviors. When $u = \bar{u}$ and $v = \bar{v}$ (Z_2 symmetric case without chirality), the model becomes equivalent to the BAW model [12]. It is solvable exactly [13] and the kink density decays with $\delta = 1/2$ for all $u < 1$. Note that the NCIM is different from the so-called directed Ising model in which kinks are biased to a preferred direction [22,23].

First, we study the maximum chirality case with $\bar{u} = \bar{v} = 0$. For convenience, we refer to this case as the maximum chirality model (MCM).

The system is prepared in an antiferromagnetic state ($\cdots + - + - + - \cdots$) initially. Then, we measure the total kink density and average it over N_S samples to obtain $\rho(t)$ for $t \leqslant 10^7$. Figure 1(a) shows the numerical data. The system sizes are $N \geqslant 2^{21}$ and the number of runs is $N_S = 5000$ for all u. The system sizes are large enough that the relaxation time scales are much larger than the simulation time. Hence, the data are free from a finite size effect. Just like the BAW model, we observed $\rho(t)$ decays in a power-law fashion $\rho(t) \sim t^{-\delta}$ for all $u < 1$. Interestingly, the scaling exponent δ seems to vary with u.

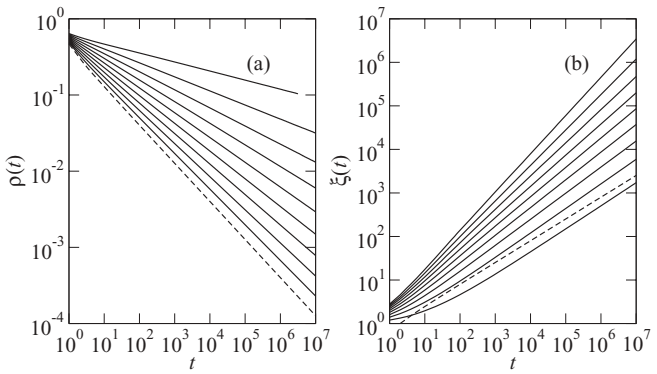

FIG. 1. Plots of $\rho(t)$ in (a) and $\xi(t)$ in (b). Dashed curves are for $u = 0.0$ while solid curves are for $u = 0.1, 0.2, \ldots, 0.9$ from bottom to top.

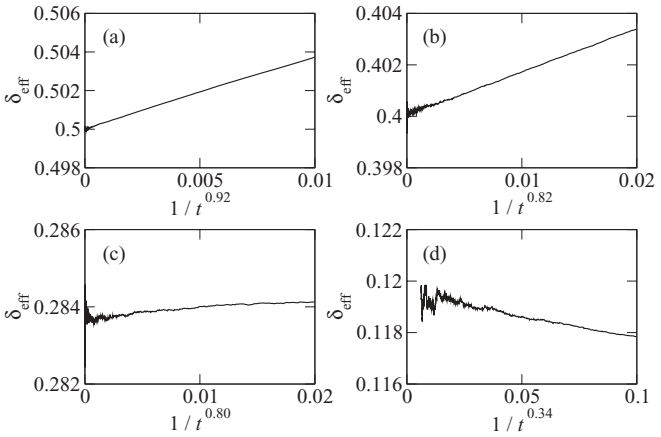

FIG. 2. Plots of effective exponents δ_{eff} for (a) $u = 0$, (b) 0.3, (c) 0.6, and (d) 0.9.

In order to estimate the scaling exponent δ precisely, we investigate the behavior of an effective exponent defined as

$$\delta_{\text{eff}}(t) = -\log[\rho(t)/\rho(t/b)]/\log b, \tag{4}$$

with a constant $b = 10$. A power-law scaling implies that the effective exponent is constant and equal to the scaling exponent. However, due to a correction-to-scaling behavior such as, e.g., $\rho(t) \simeq t^{-\delta}(a + ct^{-\zeta})$ with a leading correction-to-scaling exponent ζ, it behaves as $\delta_{\text{eff}}(t) \simeq \delta + a_1 t^{-\zeta}$ in the long time limit. So when we draw δ_{eff} against $t^{-\zeta}$ with a correct value of ζ, $\delta_{\text{eff}}(t)$ should approach to δ with a finite slope as $t \to \infty$.

Figure 2 presents the behavior of the effective exponents for $u = 0$, 0.3, 0.6, and 0.9. The correction-to-scaling exponent ζ are roughly estimated from a fitting of $\delta_{\text{eff}}(t)$ to the from $\delta + a_1 t^{-\zeta}$ with three fitting parameters δ, a_1, and ζ. This procedure can be error prone and the accuracy of the estimated ζ may be questionable. For example, the fitting yields slightly different numerical values of ζ depending on the fitting interval. This contributes to a systematic error in δ. However, such a systematic error is smaller than a statistical error in $\delta_{\text{eff}}(t)$ in the large t region in all values of u. From the correction-to-scaling analysis, we can estimate the scaling exponent δ precisely and reliably. At other values of u, we also performed the same analysis. Table I summarizes thus-obtained numerical results of δ for various u's and Fig. 3 illustrates δ against u. The error bars in Table I account for the statistical uncertainty.

The intriguing feature of the MCM is that the exponent δ varies continuously with u beyond the error bars. Furthermore, as u approaches 1, δ seems to show a nontrivial power-law behavior. Indeed, if we fit δ for the region $u \geqslant 0.6$ using $\delta \approx a_2(1-u)^{\chi}$, with two fitting parameters a_2 and χ, we found that it fits the data quite well with $a_2 \approx 0.5$ and $\chi \approx 0.62 \pm 0.03$; see Fig. 3. This singular behavior of δ at $u = 1$ may be attributed to a crossover from the mean-field voter dynamics to the MCM.

When u is very close to 1 but not exactly 1, the voter dynamics which occurs with rate $v = 1 - u$ happens after many attempts of the ASEP dynamics. Since the stationary state of the ASEP is totally uncorrelated [4], the voter dynamics can happen only after all spins are distributed almost randomly.

TABLE I. Numerical values of δ and z of the MCM for various values of u. For z, we present the results from the seed simulations [z (seed)] and from the eigenspectrum analysis [z (spectrum)]. The numbers in parentheses indicate errors of the last digits.

u	δ	z (seed)	z (spectrum)
0	0.5000(1)	1.998(8)	2.0000(6)
0.1	0.4678(2)	1.877(9)	1.8789(5)
0.2	0.4346(3)	1.769(4)	1.7683(6)
0.3	0.4001(2)	1.667(2)	1.6666(6)
0.4	0.3639(5)	1.570(6)	1.5716(8)
0.5	0.3254(5)	1.483(4)	1.4818(7)
0.6	0.2837(4)	1.397(4)	1.3958(4)
0.7	0.2376(8)	1.313(6)	1.3117(8)
0.8	0.1850(8)	1.228(3)	1.227(2)
0.9	0.1195(3)	1.139(6)	1.136(5)

Hence, if we rescale the time as $\tau = (1-u)t$ and take a limit $u \to 1$ with τ kept finite, the MCM should be the same as a mean-field voter model on a complete graph. Since coarsening does not occur on a complete graph of infinite size, δ should be zero in the above-mentioned limit. Thus, there should be a crossover from the mean-field voter dynamics to the 1D MCM at $u = 1$.

We have also performed independent Monte Carlo simulations starting with a single down kink, called a seed, in the middle of an infinite lattice $(\cdots + + + - - - \cdots)$, which are generally referred to as seed simulations. We have measured the particle spreading distance $\xi(t)$ to obtain the dynamic exponent z. When $u \neq 0$, the seed branches other kinks spreading through the space. The spreading distance $\xi(t)$ is given by the distance between the rightmost kink and the leftmost kink. When $u = 0$, the seed diffuses only. So, $\xi(t)$ is taken as the distance of the seed from the starting position.

The numerical data are presented in Fig. 1(b). The number of samples for the data are $N_S = 10^6$ at $u \leqslant 0.3$, $N_S = 10^5$ at $u = 0.4, 0.5, 0.6$, $N_S = 10^4$ at $u = 0.7, 0.8$, and $N_S = 10^3$ at $u = 0.9$. We find that the spreading length scaling follows the power-law scaling $\xi(t) \sim t^{1/z}$ with the exponent z varying with u. In order to obtain the precise estimate of z, we followed the similar effective exponent analysis as done for δ. The effective

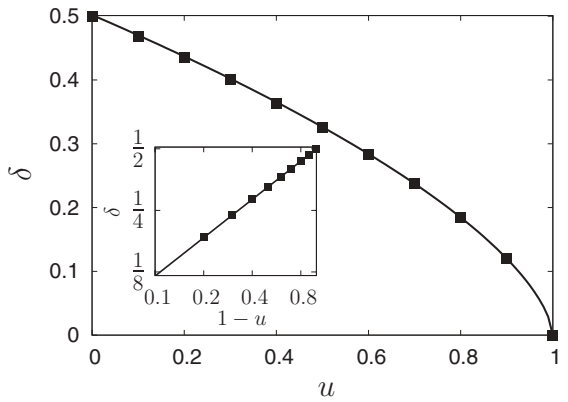

FIG. 3. Plots of δ vs u (symbols) and its fitting function $a_2(1-u)^{\chi}$ with $a_2 \approx 0.5$ and $\chi \approx 0.62$ (lines). (Inset) Log-log plot of δ against $1-u$ together with the fitting function.

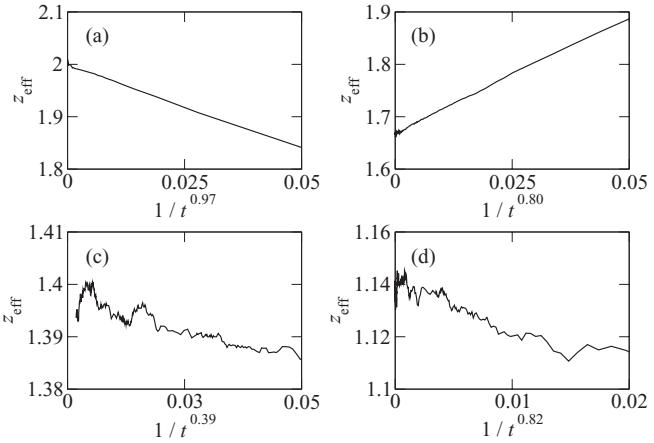

FIG. 4. Plots of effective exponents $z_{\rm eff}$ for (a) $u = 0$, (b) 0.3, (c) 0.6, and (d) 0.9.

exponent for the dynamic exponent is defined as

$$z_{\rm eff}(t) = \{\log[\xi(t)/\xi(t/b)]/\log b\}^{-1}, \tag{5}$$

with $b = 10$. Due to a correction-to-scaling behavior, $z_{\rm eff}(t)$ approaches the asymptotic scaling exponent value with a power-law correction as $z_{\rm eff}(t) = z + a' t^{-\zeta'}$ with constants a' and ζ'. Figure 4 presents the correction-to-scaling analysis result for the dynamic exponent at $u = 0, 0.3, 0.6$, and 0.9. As in the previous case, the statistical uncertainty dominates the systematic error in z. The result is summarized in Table I.

We substantiate the Monte Carlo results by studying the spectrum of the time evolution operator of the MCM. In general, a master equation can be mapped to an imaginary time Schrödinger equation with *Hamiltonian* H whose eigenvalues contain most of the relevant information of the system. For instance, the directed percolation system has been studied successfully with the eigenspectrum analysis [24–26].

For the MCM, the Hamiltonian takes the form,

$$\mathsf{H} = \frac{1}{4}\sum_{i=1}^{N}\left(1+\hat{\sigma}_i^z\right)\left(1-\hat{\sigma}_{i+1}^z\right) - u\sum_{i=1}^{N}\hat{\sigma}_i^-\hat{\sigma}_{i+1}^+ - \frac{(1-u)}{4}\sum_{i=1}^{N}\left\{\hat{\sigma}_i^-\left(1-\hat{\sigma}_{i+1}^z\right)+\left(1+\hat{\sigma}_i^z\right)\hat{\sigma}_{i+1}^+\right\}, \tag{6}$$

where $\hat{\sigma}_i$ is the Pauli spin operator acting on a spin at site i. We label eigenvalues of H as E_n with $n = 1, \ldots, 2^N$ and call E_n the energy of the nth level. Since H is not Hermitian, E_n may have a complex value. The eigenvalues are sorted in the ascending order of $\mathrm{Re}[E_n]$, the real part of E_n. There are two trivial levels with $E_1 = E_2 = 0$ corresponding to the two absorbing states with all spins having the same sign. Other low-lying energy levels with $n > 2$ define the relaxation time as $\tau_n = 1/(\mathrm{Re}[E_n])$.

We have diagonalized numerically the Hamiltonian up to $N = 20$ to obtain the longest relaxation time τ_3. Since $\tau_3 \sim N^z$, the dynamic exponent z is estimated by extrapolating an effective exponent $z_{\rm eff}(N) \equiv \ln[\tau_3(N)/\tau_3(N-2)]/\ln[N/(N-2)]$. The effective exponents are plotted in Fig. 5. The effective exponents are extrapolated using the Bulirsch-Stoer (BST) algorithm with an assumption of a power-law correction as $z_{\rm eff}(N) = z + aN^{-\omega} + \cdots$ [27,28]. The

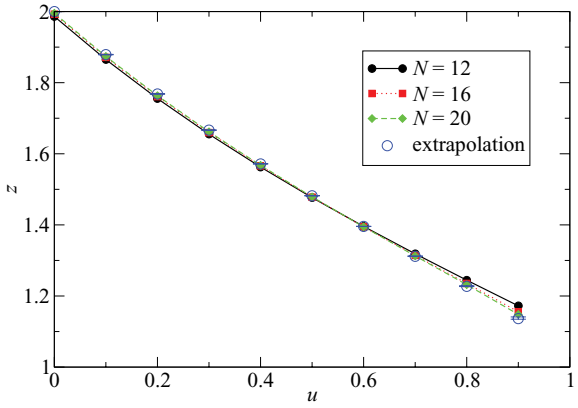

FIG. 5. (Color online) Effective exponents for the dynamic exponent z obtained from the spectrum analysis and their extrapolated estimates. Lines are guides to the eyes.

correction-to-scaling exponent ω is not known *a priori*. Hence, we apply the BST algorithm with several values of $\omega = 0.5, 1.0, \ldots, 3.0$. The numerical values for z are obtained as the average of them. Error bars are estimated as the maximum deviation between them. They are plotted in Fig. 5 and summarized in Table I. Both results for z from the spectrum analysis and from the seed simulation are in perfect agreement with each other and vary continuously with u.

We have shown that the coarsening dynamics of the MCM is characterized by continuously varying critical exponents. Note that chirality lies both in the ASEP events ($u \neq \bar{u}$) and the voter-model events ($v \neq \bar{v}$). In order to investigate which one is the essential ingredient, we studied two more cases: One is the case with $u = \bar{u}$ and $v \neq \bar{v} = 0$ which will be called the symmetric exclusion and chiral voter (SECV) model and the other is the case with $u \neq \bar{u} = 0$ and $v = \bar{v}$ to be called the chiral exclusion and symmetric voter (CESV) model. The CESV model is a particular limiting case of the model studied in Refs. [20,21]. Remind that v is always set to $1 - u$.

The analyses of $\delta_{\rm eff}$ for the SECV with $u = 0.1$, 0.2, 0.5, and 0.8 are summarized in Fig. 6. It seems that $\delta_{\rm eff}(t)$ for all u approaches $1/2$ with logarithmic corrections. Notice that if there exists a logarithmic correction as

$$\rho(t) \sim (\ln t + C)^{\kappa}/t^{\delta}, \tag{7}$$

with a constant C, the effective exponent defined in Eq. (4) should behave as $\delta_{\rm eff}(t) \approx \delta - \kappa/\ln t$ in the asymptotic regime. Thus, if we plot $\delta_{\rm eff}(t)$ as a function of $1/\ln t$, the effective exponent should intersect the y axis with slope $-\kappa$. This phenomenon is quite pronounced for the cases of $u = 0.5$ and 0.8 and the slope seems to be around 0.5. Indeed, if $\rho(t)\sqrt{t}/(\ln t)^{0.53}$ is plotted against t on a semilogarithmic scale (see inset of Fig. 6 for the case of $u = 0.8$), a flat region is observable in the long time limit for more than two log decades. Although the accurate value of κ is hard to estimate, we can conclude that there exists a systematic logarithmic correction as shown in Eq. (7) with the leading scaling exponent $\delta = 1/2$ unchanged in the SECV model.

A logarithmic correction in a 1D coarsening has been reported in a different model [14] that corresponds to the voter model with a weak kinetic constraint. In that model, the kink density decays faster than $1/\sqrt{t}$ as $1/(\sqrt{t}\ln t)$, but in our case

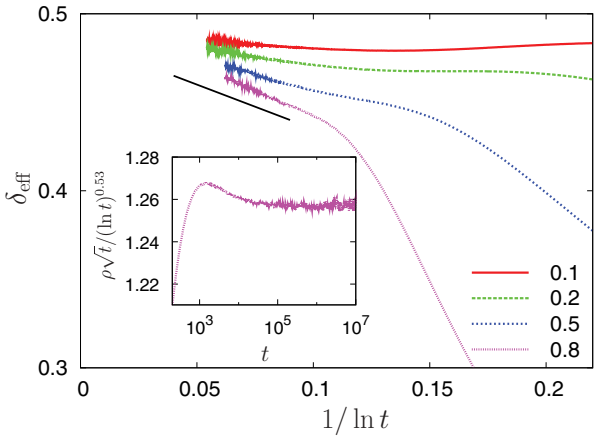

FIG. 6. (Color online) Plots of $\delta_{\rm eff}$ as functions of $1/\ln t$ for $u = 0.1$, 0.2, 0.5, and 0.8 (from top to bottom) for the SECV. A line segment with slope -0.5 is for a guide to the eyes. (Inset) Plot of $\rho(t)\sqrt{t}/(\ln t)^{0.53}$ vs t for the SECV with $u = 0.8$ on a semilogarithmic scale.

it decays slower than $1/\sqrt{t}$. Qualitatively, this slowing down should be attributed to the presence of branching dynamics which increases the number of kinks. However, a quantitative analysis requires further investigation, which is beyond the scope of this paper. For our purpose, it is enough to conclude that the continuously varying exponents are not due to the chiral voter dynamics.

The CESV model shows a more intriguing feature. We present the effective exponent data for the density decay in Fig. 7. For $u = 0.2$ [Fig. 7(a)], $\delta_{\rm eff}$ seems to approach 0.5 with negligible logarithmic correction. For $u = 0.5$ [Fig. 7(b)], we cannot make a firm conclusion whether $\delta < 0.5$ or $\delta = 0.5$ due to strong correction-to-scaling behavior. Quite interestingly, when $u > 0.5$ [Figs. 7(c) and 7(d)], δ deviates from 0.5 significantly even under the assumption of a logarithmic correction. So we conclude that the CESV has continuously varying exponents with possible logarithmic corrections when

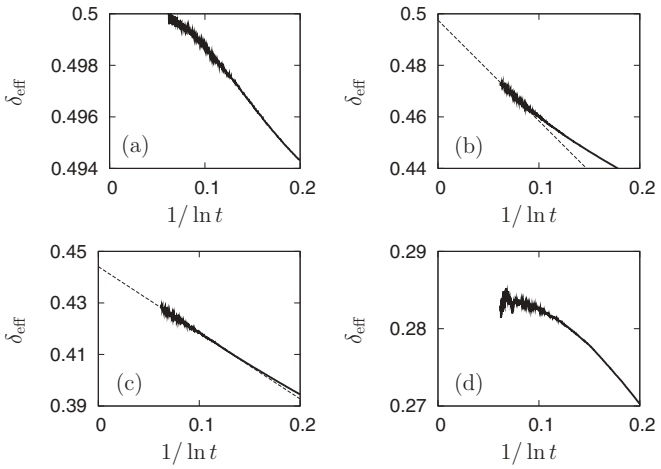

FIG. 7. Plots of $\delta_{\rm eff}$ as functions of $1/\ln(t)$ for $u =$ (a) 0.2, (b) 0.5, (c) 0.6, and (d) 0.8 for the CESV. For the case of $u = 0.5$ and 0.6 [(b) and (c)], fitting results of a function $\delta + d/\ln t$ with δ and d fitting parameters are also depicted.

$u > 0.5$. This study shows that the chirality in the spin exchange is responsible for the continuously varying exponents. Nevertheless, it remains open why and when there appears a logarithmic correction in the coarsening process.

To summarize, we have studied the one-dimensional coarsening dynamics of nonequilibrium Ising spin systems with chirality. Although chirality is irrelevant in equilibrium Ising systems, it turns out that the chirality can lead to continuously varying scaling exponents in the nonequilibrium chiral Ising model. In particular, it turns out that the chirality in spin exchange plays a crucial role.

It is rare to observe continuously varying exponents from systems without quenched disorder. The q-state Potts model with zero-temperature Glauber dynamics was studied in Refs. [8,9]. It was found that the critical exponent describing the power-law decay of the persistent probability varies continuously with q. Nevertheless, the coarsening dynamics is still pure diffusive and characterized by $z = 2$ and $\delta = 1/2$ at all values of q. We notice that continuously varying exponents were reported in a 1D sandpile model without dissipation [29] and that there is actually a parallelism between this sandpile model and the MCM. This connection will be discussed elsewhere [30].

Some of Ising spin systems are exactly solvable in one dimension [2,5,8,25], for equations governing the time evolution of correlation functions are closed. In the presence of the chirality, however, the equations are not closed, which makes the exact solution for the NCIM not available in general. Our numerical finding of the universality class with continuously varying exponents can be established more firmly if one finds a minimal continuum equation obeying the proper symmetry property. We leave it as a future work [30].

This work was supported by the National Research Foundation of Korea (NRF) grant funded by the Korea government, Ministry of Education, Science and Technology (MEST) (Grant No. 2012-0005003). S.-C.P. acknowledges support from the Basic Science Research Program through NRF funded by MEST (Grant No. 2011-0014680). M.K. acknowledges financial support from the TJ Park Foundation. Discussion with J. Krug, B. Derrida, and G. Schütz is appreciated. The computation was partly supported by Universität zu Köln.

[1] A. J. Bray, Adv. Phys. **51**, 481 (2002).
[2] R. J. Glauber, J. Math. Phys. **4**, 294 (1963).
[3] K. Kawasaki, Phys. Rev. **145**, 224 (1966).
[4] T. M. Liggett, *Interacting Particle Systems* (Springer-Verlag, New York, 1995).
[5] J. T. Cox, Ann. Probab. **17**, 1333 (1989).
[6] J. G. Amar and F. Family, Phys. Rev. A **41**, 3258 (1990).
[7] C. Sire and S. N. Majumdar, Phys. Rev. E **52**, 244 (1995).
[8] B. Derrida, V. Hakim, and V. Pasquier, Phys. Rev. Lett. **75**, 751 (1995).
[9] B. Derrida and R. Zeitak, Phys. Rev. E **54**, 2513 (1996).
[10] I. Dornic, H. Chaté, J. Chave, and H. Hinrichsen, Phys. Rev. Lett. **87**, 045701 (2001).
[11] N. Menyhárd, J. Phys. A **27**, 6139 (1995).
[12] H. Takayasu and A. Y. Tretyakov, Phys. Rev. Lett. **68**, 3060 (1992).
[13] D. ben-Avraham, F. Leyvraz, and S. Redner, Phys. Rev. E **50**, 1843 (1994).
[14] S. N. Majumdar, D. S. Dean, and P. Grassberger, Phys. Rev. Lett. **86**, 2301 (2001).
[15] T. Vicsek, A. Czirók, E. Ben-Jacob, I. Cohen, and O. Shochet, Phys. Rev. Lett. **75**, 1226 (1995).
[16] G. Grégoire and H. Chaté, Phys. Rev. Lett. **92**, 025702 (2004).
[17] T. Vicsek, A. Czirok, I. J. Farkas, and D. Helbing, Physica A **274**, 182 (1999).
[18] I. D. Couzin and N. R. Franks, Proc. R. Soc. Lond. B **270**, 139 (2003).
[19] S. Ostlund, Phys. Rev. B **24**, 398 (1981).
[20] V. Belitsky, P. A. Ferrari, M. V. Menshikov, and S. Y. Popov, Bernoulli **7**, 119 (2001).
[21] I. M. MacPhee, M. V. Menshikov, S. Volkov, and A. R. Wade, Bernoulli **16**, 1312 (2010).
[22] C. Godrèche and A. J. Bray, J. Stat. Mech. (2009) P12016.
[23] C. Godrèche, J. Stat. Mech. (2011) P04005.
[24] M. Henkel and H. J. Herrmann, J. Phys. A **23**, 3719 (1990).
[25] D. ben-Avraham, R. Bidaux, and L. S. Schulman, Phys. Rev. A **43**, 7093 (1991).
[26] E. Carlon, M. Henkel, and U. Schollwöck, Eur. Phys. J. B **12**, 99 (1999).
[27] R. Bulirsch and J. Stoer, Numer. Math. **6**, 413 (1964).
[28] M. Henkel and G. Schütz, J. Phys. A **21**, 2617 (1988).
[29] K. Jain, Europhys. Lett. **71**, 8 (2005).
[30] M. Kim, J. D. Noh, and S.-C. Park (unpublished).